BIOLOGICAL CRYSTALLOGRAPHY

ISSN 1399-0047

An enzyme captured in two conformational states: crystal structure of *S*-adenosyl-L-homocysteine hydrolase from *Bradyrhizobium elkanii*

Tomasz Manszewski,[a] Kriti Singh,[a] Barbara Imiolczyk[a] and Mariusz Jaskolski[a,b]*

[a]Center for Biocrystallographic Research, Institute of Bioorganic Chemistry, Polish Academy of Sciences, Poznan, Poland, and [b]Department of Crystallography, Faculty of Chemistry, A. Mickiewicz University, Poznan, Poland. *Correspondence e-mail: mariuszj@amu.edu.pl

Received 7 August 2015
Accepted 5 October 2015

Edited by Z. Dauter, Argonne National Laboratory, USA

Keywords: nitrogen fixation; plant–bacteria interactions; *S*-adenosyl-L-homocysteine; *S*-adenosyl-L-homocysteine hydrolase; *S*-adenosyl-L-methionine; adenosine; homocysteine; nicotinamide adenine dinucleotide.

PDB reference: *S*-adenosyl-L-homocysteine hydrolase, complex with adenosine, 4lvc

Supporting information: this article has supporting information at journals.iucr.org/d

S-Adenosyl-L-homocysteine hydrolase (SAHase) is involved in the enzymatic regulation of *S*-adenosyl-L-methionine (SAM)-dependent methylation reactions. After methyl-group transfer from SAM, *S*-adenosyl-L-homocysteine (SAH) is formed as a byproduct, which in turn is hydrolyzed to adenosine (Ado) and homocysteine (Hcy) by SAHase. The crystal structure of BeSAHase, an SAHase from *Bradyrhizobium elkanii*, which is a nitrogen-fixing bacterial symbiont of legume plants, was determined at 1.7 Å resolution, showing the domain organization (substrate-binding domain, NAD^+ cofactor-binding domain and dimerization domain) of the subunits. The protein crystallized in its biologically relevant tetrameric form, with three subunits in a closed conformation enforced by complex formation with the Ado product of the enzymatic reaction. The fourth subunit is ligand-free and has an open conformation. The BeSAHase structure therefore provides a unique snapshot of the domain movement of the enzyme induced by the binding of its natural ligands.

1. Introduction

S-Adenosyl-L-methionine (SAM) is used in the vast majority of enzymatic methylation reactions because of its methyl-group transfer potential (Cantoni, 1975; Richards *et al.*, 1978). SAM acts as the methyl-donor substrate in the methylation of a large variety of biological molecules, ranging from macromolecules such as proteins, nucleic acids and polysaccharides to small molecules such as catecholamines, histamines and norepinephrine (Keller & Borchardt, 1988). Upon methyl-group transfer, SAM is converted to *S*-adenosyl-L-homocysteine (SAH). This byproduct of methylation is a strong inhibitor of SAM-dependent methyltransferases (Chiang & Cantoni, 1979; Cantoni & Chiang, 1980; Liu *et al.*, 1992) and must be enzymatically decomposed to adenosine (Ado) and homocysteine (Hcy) by *S*-adenosyl-L-homocysteine hydrolase (SAHase; De la Haba & Cantoni, 1959). Thus, by maintaining the appropriate SAM:SAH ratio, SAHase serves as an important regulator of cellular SAM-dependent methyltransferases. Plant SAHases have also been implicated in cytokinin binding (Mitsui *et al.*, 1993), but in view of the recent structural studies of SAHase from yellow lupin (Brzezinski *et al.*, 2012) this hypothesis is probably not true, as the N6 substituent of cytokinins would generate steric clashes with the adenine-binding site of the protein

The equilibrium of the SAH hydrolysis reaction lies far in the direction of substrate synthesis; however, under physiological conditions the products, Ado and Hcy, are quickly removed (Richards *et al.*, 1978). Ado is converted to inosine or

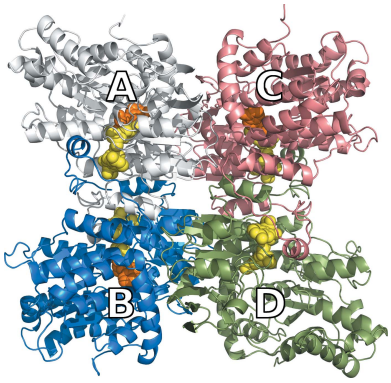

adenosine triphosphate by adenosine deaminase (ADA) or adenosine kinase (AK), respectively. It has been shown that accumulation of Ado causes inhibition of SAHase, which in turn leads to combined immune deficiency (Kredich & Martin, 1977; Hershfield & Kredich, 1978; Hershfield, 1979; Hershfield *et al.*, 1979). Hcy is used in remethylation and transsulfuration reactions in an approximately 1:1 ratio (Robinson *et al.*, 1994). Remethylation leads to methionine regeneration *via* two different pathways. One of them is irreversible, takes place in the liver and kidneys and involves betaine (McKeever *et al.*, 1991), while the more important one requires a methyl-group transfer to Hcy from 5-methyltetrahydrofolate by 5-methyltetrahydrofolate homocysteine methyltransferase in the folate cycle. It has been shown that an elevated plasma level of Hcy is a risk factor in coronary heart disease (Nygård *et al.*, 1997).

SAHases are usually active as tetramers, with the only exception being plant SAHases, which function as homodimers (Guranowski & Pawełkiewicz, 1977; Brzezinski *et al.*, 2008). The SAHase subunit is comprised of ∼420 (for archaeal and some bacterial enzymes) or ∼480 (for most eukaryotic and bacterial enzymes) residues and has a molecular weight of about 45–55 kDa. This difference is owing to the presence of an ∼40-residue insert in the latter group of SAHases (Stępkowski *et al.*, 2005). In each subunit there is one tightly but noncovalently bound molecule of the NAD^+ cofactor, which is required for enzymatic activity (Palmer & Abeles, 1979; Fujioka & Takata, 1981). Each subunit consists of two main domains, the substrate-binding domain and the cofactor-binding domain, and a small C-terminal dimerization domain.

SAHases can exist in two different conformations described as open and closed. The difference between these two states is in the relative position of the substrate-binding and cofactor-binding domains. In the open conformation, which is characteristic of the substrate/product-free enzyme, the domains are swung apart and the active site is accessible. The opposite situation occurs when the active site is occupied by a ligand molecule: the main domains come close together, adopting the closed conformation.

The mechanism of the reaction catalyzed by SAHase, described by Palmer & Abeles (1976, 1979), can be briefly summarized as follows. Firstly, SAH is oxidized to a 3′-keto derivative with NAD^+ as the oxidant. The 4′ proton is then abstracted by the N^{ζ} atom of a lysine located in the active site and the Hcy moiety at the 5′ position is eliminated, leading to 3′-keto-4′,5′-dehydroadenosine. The last step is Michael addition of a water molecule and reduction of the 3′-keto derivative to adenosine with simultaneous conversion of NADH to NAD^+.

The crystal structures of several SAHases are known, including mammalian [*Homo sapiens* (Turner *et al.*, 1998, PDB entry 1a7a; Yang *et al.*, 2003, PDB entry 1li4), *Rattus norvegicus* (Hu *et al.*, 1999, PDB entry 1b3r; Huang *et al.*, 2002, PDB entry 1k0u; Takata *et al.*, 2002, PDB entry 1ky5)], plant [*Lupinus luteus* (Brzezinski *et al.*, 2012, PDB entries 3ond, 3one and 3onf)], protozoan [*Plasmodium falciparum* (Tanaka *et al.*, 2004, PDB entry 1v8b), *Trypanosoma brucei* (Structural Genomics Consortium, unpublished work, PDB entry 3h9u)] and bacterial [*Mycobacterium tuberculosis* (Reddy *et al.*, 2008, PDB entry 3ce6), *Burkholderia pseudomallei* (Seattle Structural Genomics Center for Infectious Disease, unpublished work, PDB entry 3d64), *Brucella melitensis* (unpublished work, PDB entry 3n58)] proteins. Here, we present the first crystal structure of SAHase from a nodulating bacterium, *Bradyrhizobium elkanii* (BeSAHase), in complex with the reaction product adenosine (Ado). Nodulating bacteria colonize the root nodules of legume plants in a symbiotic association that leads to atmospheric nitrogen fixation. Together with the structure of the enzyme from a legume plant (LlSAHase; Brzezinski *et al.*, 2012), the structure of BeSAHase also provides the first example of a pair of orthologous enzymes from symbiotic partners for structural comparison.

The plant–bacteria symbiosis, leading to the formation of nodules and allowing atmospheric nitrogen fixation by plants, starts with the activation of bacterial genes responsible for the biosynthesis of Nod factor (NF). One of the NF modification enzymes, NodS, is a SAM-dependent methyltransferase and its activity is controlled by a SAHase, which maintains the appropriate SAM:SAH ratio.

2. Materials and methods

2.1. Cloning, overexpression and purification

The coding sequence of SAHase was amplified from a *B. elkanii* cDNA library by PCR and cloned into the pET151/D-TOPO plasmid, which adds a His_6 tag at the N-terminus of the expressed sequence. The vector was used to transform the BL21 Star (DE3) strain of *E. coli*. 6 l of LB medium containing 100 µg ml^{-1} ampicillin was inoculated with 150 ml of overnight culture and grown at 310 K to an OD_{600} of 1.0. The culture was induced with IPTG at a final concentration of 0.4 m*M*. The cells were harvested after 4 h of induction by centrifugation, the supernatant was removed and the cell pellet was resuspended in buffer *A* consisting of 50 m*M* Tris pH 8.0, 500 m*M* NaCl, 20 m*M* imidazole. The cells were disrupted by pulse sonication on ice and centrifuged. The supernatant was loaded onto an Ni–NTA affinity column and the protein was eluted with 15 ml buffer *B* (50 m*M* Tris pH 8.0, 500 m*M* NaCl, 300 m*M* imidazole). The protein concentration was estimated to be 8 mg ml^{-1} according to Bradford (1976). SDS–PAGE analysis confirmed that the molecular weight of the expressed protein was ∼52 kDa. Following elution, the protein was dialyzed against buffer *A*. 100 µg of TEV protease per milligram of protein was added to remove the His tag. After 20 h incubation, the protein solution was again loaded onto the nickel-affinity column to remove the His-tag debris and His-tagged TEV protease. The purified protein was loaded onto a desalting column equilibrated with buffer *C* (20 m*M* Tris pH 8.0, 50 m*M* NaCl). To ensure the presence of the cofactor in the uniformly oxidized state, NAD^+ was added (as the sodium salt) in a 12-fold molar excess and the mixture was incubated for 3 h on ice. Finally, the protein solution was loaded onto a gel-filtration column equilibrated with buffer *C*.

Table 1
Data-collection and structure-refinement statistics.

Values in parentheses are for the last resolution shell.

Data collection	
Beamline	14.1, BESSY
Wavelength (Å)	0.918
Temperature (K)	100
Crystal system	Orthorhombic
Space group	$P2_12_12$
Unit-cell parameters (Å)	a = 107.7, b = 176.5, c = 104.3
Mosaicity (°)	0.23
Resolution range (Å)	47.85–1.74 (1.79–1.74)
Total reflections	1278402
Unique reflections	200549
Multiplicity	6.4 (4.2)
Completeness (%)	98.7 (97.0)
$\langle I/\sigma(I)\rangle$	12.34 (1.95)
$R_{\rm merge}$†	0.086 (0.694)
Refinement	
No. of working/test reflections	199538/1011
$R/R_{\rm free}$‡	0.148/0.172
No. of protein atoms	14468
No. of Ado atoms	57
No. of NAD^+ atoms	176
No. of water atoms	1704
No. of NH_4^+ ions	3
No. of acetate ions	3
No. of glycerol molecules	15
$\langle B\rangle$ (Å^2)	
Protein	27.1
Ado	29.3
NAD^+	21.3
Solvent	39.4
R.m.s.d. from ideality for bonds (Å)	0.018
Ramachandran statistics	
Favoured (%)	97.2
Allowed (%)	2.8
PDB code	4lvc

† $R_{\rm merge} = \sum_{hkl}\sum_i |I_i(hkl) - \langle I(hkl)\rangle| / \sum_{hkl}\sum_i I_i(hkl)$, where $\langle I(hkl)\rangle$ is the average intensity of reflection hkl. ‡ $R = \sum_{hkl} ||F_{\rm obs}| - |F_{\rm calc}|| / \sum_{hkl} |F_{\rm obs}|$, where $F_{\rm obs}$ and $F_{\rm calc}$ are the observed and calculated structure factors, respectively. $R_{\rm free}$ is calculated analogously for the test reflections, which were randomly selected and excluded from refinement.

Fractions containing BeSAHase were collected, concentrated to 12 mg ml^{-1} and used for crystallization.

2.2. Crystallization

Single crystals suitable for diffraction experiments were obtained in condition No. 30 of the PEG/Ion screen (Hampton Research), consisting of 0.2 *M* ammonium acetate, 20%(*w*/*v*) polyethylene glycol 3350 pH 7.1. Crystallization was conducted by vapour diffusion in hanging drops at 292 K.

2.3. Data collection, structure solution and refinement

Low-temperature X-ray diffraction data extending to 1.74 Å resolution were collected on beamline 14.1 at BESSY at a wavelength of 0.918 Å. 20%(*v*/*v*) glycerol was used as a cryoprotectant. The crystals belonged to the orthorhombic system with space group $P2_12_12$. The diffraction data were processed and scaled with *XDS* (Kabsch, 2010) as summarized in Table 1.

The structure was solved by molecular replacement using *Phaser* (McCoy *et al.*, 2007). The atomic coordinates of chain *A* of SAHase from *B. melitensis* (PDB entry 3n58) served as the search model. The search procedure found four copies (labelled *A*, *B*, *C* and *D*) of the model chain arranged into a tetrameric assembly, which was built with the correct sequence using the *ARP*/*wARP* server (Langer *et al.*, 2008). The model was refined in *REFMAC*5 (Murshudov *et al.*, 2011) with maximum-likelihood targets. Three groups of TLS parameters (Painter & Merritt, 2006) were used per subunit. *Coot* (Emsley & Cowtan, 2004) was used for manual model rebuilding between rounds of refinement. A test refinement without planarity restraints for the nicotinamide moiety of the NAD^+ molecule was calculated to probe the oxidation state of the cofactor. The final structure-refinement statistics are shown in Table 1.

The polypeptide chain of BeSAHase is comprised of 473 amino-acid residues. The construct used in this work has six extra residues (GIDPFT–) at the N-terminal end that were introduced by the cloning vector. However, in the crystal structure these extra residues plus the first five genuine residues of the protein (–MNAKP–) were not modelled in the electron density because of disorder. Difference Fourier maps clearly indicated the presence of one NAD^+ cofactor molecule in each subunit. 1704 water molecules, 15 glycerol molecules, three acetate ions and three ammonium ions (the latter found only in the subunits complexed with Ado) were also modelled in the electron-density maps. During the analysis of difference Fourier maps, clear electron density corresponding to three adenosine (Ado) molecules was detected in subunits *A*, *B* and *C*.

The stereochemical restraints for the protein chains were as defined in *REFMAC*, while the restraint libraries for the Ado and NAD^+ ligands were built in *elBOW* (Moriarty *et al.*, 2009) as implemented in *PHENIX* (Adams *et al.*, 2010).

The *PyMOL* molecular-graphics system (DeLano, 2002) was used to prepare all of the figures presented in this paper.

3. Results and discussion

3.1. Overall structure of BeSAHase

The enzyme crystallizes as a 222 pseudosymmetric homotetramer (Fig. 1), with each subunit composed of 473 amino-acid residues, of which residues 6–473 are well ordered and could be modelled in the electron density. Each protomer consists of two large domains, the substrate-binding domain and the cofactor-binding domain, which are separated by a deep crevice forming the substrate-access channel to the active site, and a small C-terminal oligomerization domain.

The substrate-binding domain, built from amino-acid residues Gly6–Val221 and Met397–Val426, has an α/β-fold. The central parallel β-sheet is built from seven β-strands with the following topology: −1x, −1x, +3x, +1x, +1x, +1x. The cofactor-binding domain is comprised of residues Tyr234–Gly391 and has an unusual Rossmann fold, with the central mixed β-sheet composed of eight β-strands with topology +1x, +1x, −3x, −1x, −3x, +1, +1 as in previously reported SAHase structures (Brzezinski *et al.*, 2012). These two main domains are joined by two hinge regions built from amino-acid residues

Asn222–Leu233 and His392–Val396. The C-terminal domain, formed by residues Leu427–Tyr473, has a helix–loop–helix–loop fold. This domain is located away from the catalytic region of its own subunit (*e.g.* *A*) and is inserted in a mutual fashion into the cofactor-binding domain of an adjacent subunit (*B*). The mutual swapping of the C-terminal domains between pairs of subunits leads to their discernible tight dimerization. The tetrameric enzyme molecule must therefore be considered as a dimer of intimate dimers.

The centre of the tetramer is formed by the cofactor-binding domains, while the substrate-binding domains are located outside the core of the enzyme, where they are much more mobile than the rigid central part.

3.2. The adenosine molecules

Upon inspection of the difference Fourier maps, clear electron density corresponding to three adenosine molecules was identified (Fig. 2*a*) in subunits *A*, *B* and *C*, which are in a closed conformation (see §3.4), even though the nucleoside was not added at any stage of protein purification or crystallization. The identification of the unknown molecule as Ado was straightforward, as the location, conformation and protein interactions of this ligand in the substrate-binding domain were known to us from our previous studies of the LlSAHase–Ado complex (Brzezinski *et al.*, 2012).

During the refinement and electron-density modelling, the occupancy of the three Ado molecules was adjusted to 0.7. The incomplete saturation of the Ado-binding sites is explained by the fact the ligand was sequestered from the limited pool available in the bacterial cell during the high-level overexpression of the recombinant protein.

The binding mode of the Ado molecules is similar to those observed in previously reported structures containing Ado or its analogues (Turner *et al.*, 1998; Tanaka *et al.*, 2004; Reddy *et al.*, 2008). The Ado-binding site is situated in the crevice between the substrate-binding and cofactor-binding domains. The Ado molecules interact with amino-acid residues from both the substrate-binding and cofactor-binding domain, and are stabilized in the active site by a number of hydrogen bonds and hydrophobic interactions. The hydrogen bonds are formed with the participation of both the main chain and side chains of the protein (Table 2) using all of the heteroatoms of

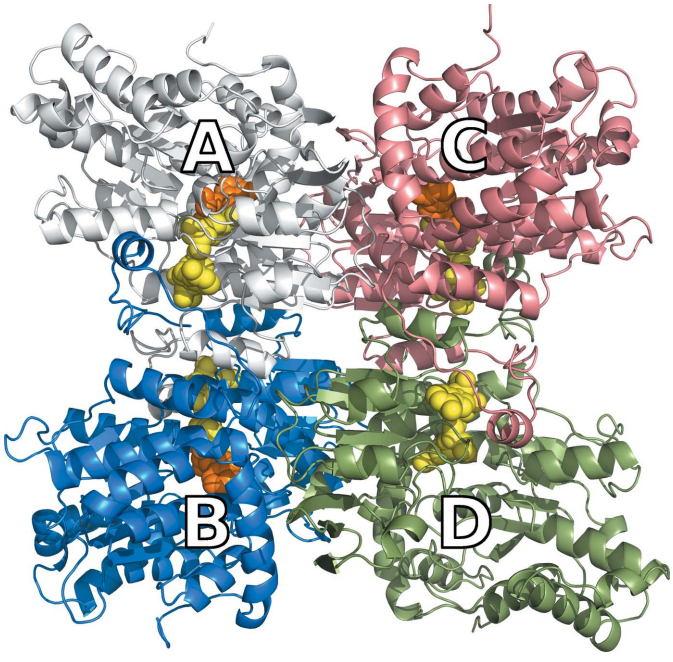

Figure 1
A ribbon diagram of the BeSAHase tetramer, with the subunits labelled *A*, *B*, *C* and *D*. The NAD^+ (yellow) and adenosine (orange) molecules are shown in space-filling representation. The pseudodyad relating the subunits of the intimate dimers (*AB* and *CD*) is horizontal in this view. The remaining axes of the 222 pseudosymmetric tetramer are vertical and perpendicular to the paper.

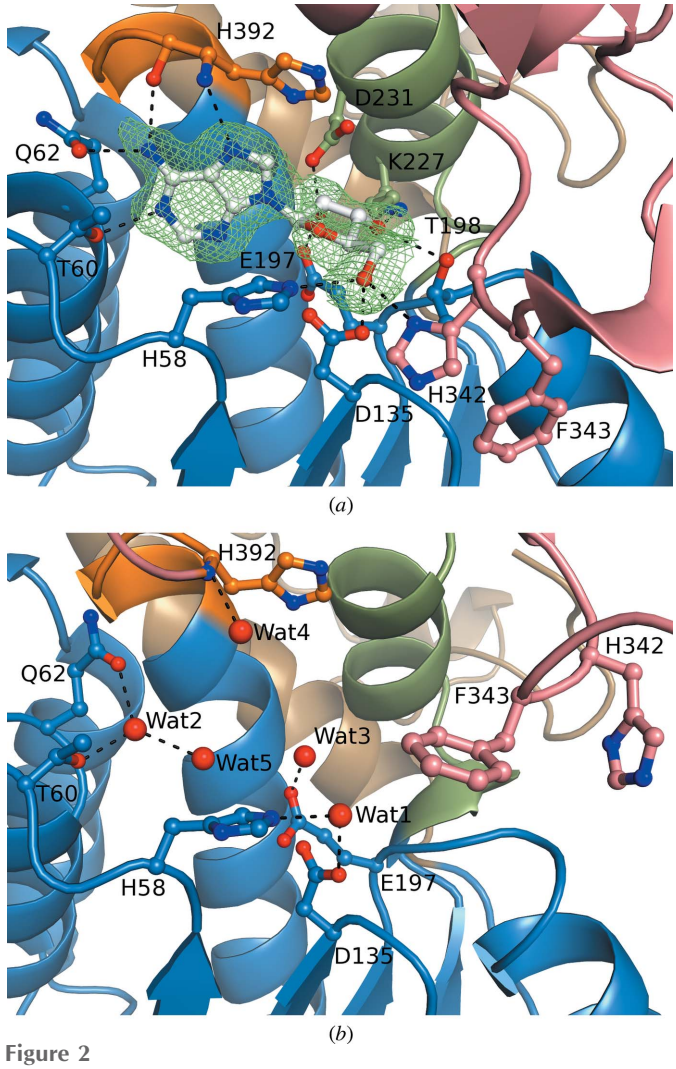

Figure 2
Comparison of the active site in subunit *A* (closed form) (*a*) and subunit *D* (open form) (*b*). The Ado molecule in (*a*) is shown in an $F_o - F_c$ OMIT electron-density map (calculated without the contribution of the Ado atoms to F_c) contoured at the 3σ level (corresponding to 0.17 e Å^{-3}). Water molecules in (*b*) are represented as red spheres. Dashed lines represent the hydrogen bonds listed in Table 2. The different domains of the BeSAHase subunit are highlighted by colours: blue, substrate-binding domain; salmon, cofactor-binding domain; sand, C-terminal domain. Green and orange colours represent, respectively, the first and second hinge regions between the substrate-binding and cofactor-binding domains.

Table 2
Hydrogen bonds between the Ado molecules bound in subunits *A*/*B*/*C* and protein atoms.

For comparison, the contacts of the corresponding residues from subunit *D* are also shown.

Residue No. and atom	Ado atom	Distance (Å)	Interactions in subunit *D*
His58 $N^{\varepsilon 2}$	O4′	3.17/3.08/3.22	No interaction
His58 $N^{\varepsilon 2}$	O5′	2.86/2.76/2.86	Water(1)
Thr60 $O^{\gamma 1}$	N1	2.76/2.74/2.73	Water(2)
Gln62 $O^{\varepsilon 1}$	N6	2.82/3.01/2.95	Water(2)
Asp135 $O^{\delta 1}$	O5′	2.90/2.82/2.87	Water(1)
Glu197 $O^{\varepsilon 2}$	O2′	2.65/2.80/2.59	Water(3)
Thr198 $O^{\gamma 1}$	O3′	3.21/2.98/3.05	No interaction
Lys227 N^{ζ}	O3′	2.69/2.82/2.79	No interaction
Asp231 $O^{\delta 1}$	O2′	2.72/2.51/2.70	No interaction
His342 $N^{\delta 1}$	O5′	2.73/2.81/2.68	No interaction
His392 N	N7	2.86/2.88/2.99	Water(4)
His392 O	N6	3.07/3.09/3.01	No interaction

the Ado molecules except N3. The purine N6 atom is a donor of two hydrogen bonds to the His392 O atom, which is also involved in the coordination of the ammonium ion, and the Gln62 $O^{\varepsilon 1}$ atom. These hydrogen bonds indicate that the adenine moiety is in the amino rather than the imino form. The ribose ring has a strained O4′-*endo* conformation, stabilized by two hydrogen bonds between the 3′-hydroxyl and the Thr198 $O^{\gamma 1}$ and Lys227 N^{ζ} atoms.

A comparison with the Ado molecules bound to SAHase from *L. luteus* (Brzezinski *et al.*, 2012) reveals a high level of similarity of the conformational parameters, such as the *anti* orientation of the adenine ring around the glycosidic bond and the relative orientation of the O5′ atom against the ribose moiety, described by the C3′—C4′—C5′—O5′ torsion angle (γ), which is *trans*. Full conformational details of the Ado nucleosides, including the pseudorotation parameters of the ribofuranose rings, are listed in Table 3.

3.3. The adenosine-binding site in the ligand-free subunit

The active site of the ligand-free subunit *D* cannot be overlaid directly on those of subunits *A*, *B* and *C* in the closed conformation because the corresponding residues are too far apart. In general, the area occupied by Ado in subunit *A* is filled with five water molecules in subunit *D*. Four of these solvent molecules mimic the positions of Ado heteroatoms and therefore create a similar pattern of hydrogen bonds to the same amino-acid residues (Fig. 2*b*).

The position of the O5′ atom of the Ado molecule is mimicked in subunit *D* by a water molecule [Water(1) in Table 2] hydrogen-bonded to the His58 $N^{\varepsilon 2}$ and Asp135 $O^{\delta 1}$ atoms, which in subunit *A* interact with O5′. In the active sites occupied by Ado, there is also a hydrogen bond between O5′ and His342 $N^{\delta 1}$, but His342, which is an element of the 'molecular gate' (see §3.5), in subunit *D* does not interact with Water(1) as it changes conformation completely to open the access to the empty active site (see below). The second water molecule [Water(2)] occupies the position corresponding to N1 of Ado and likewise creates a hydrogen bond to the $O^{\gamma 1}$ atom of Thr60 and additionally to Gln62 $O^{\varepsilon 1}$. This solvent

Table 3
Conformation of the Ado molecules found in subunits *A*, *B* and *C*.

The amplitude (τ_m) and phase angle (*P*) of pseudorotation were calculated by the method of Jaskólski (1984).

	Adenosine (*A*)	Adenosine (*B*)	Adenosine (*C*)
Glycosidic bond	*Anti*	*Anti*	*Anti*
Angle (°)†			
χ	−117.1	−106.7	−119.8
γ	−177.9	−179.1	−167.7
ν_0	−40.0	−28.1	−42.7
ν_1	18.5	11.2	19.0
ν_2	7.8	7.8	9.5
ν_3	−31.2	−24.3	−34.9
ν_4	45.8	33.9	49.8
P	79.8 (10)	75.8 (11)	78.4 (9)
τ_m	45.0 (8)	32.9 (7)	48.8 (8)
Sugar pucker	O4′-*endo* ($^0T_4$)	O4′-*endo* ($^0T_4$)	O4′-*endo* ($^0T_4$)

† The torsion angles defining the nucleoside conformation are as follows: χ, C4—N9—C1′—O4′; γ, O5′—C5′—C4′—C3′; ν_0, C4′—O4′—C1′—C2′; ν_1, O4′—C1′—C2′—C3′ *etc.*

Table 4
R.m.s. deviations (Å) for C^{α} atoms of superposed subunits of BeSAHase.

Values were calculated with *ALIGN* (Cohen, 1997).

Subunit	*A*	*B*	*C*
B	0.20		
C	0.12	0.21	
D	2.32	2.28	2.26

molecule also interacts *via* a hydrogen bond with another water molecule [Water(5)], which occupies the position of the N3 Ado atom, although the N3 atom itself does not form any hydrogen bonds to the enzyme (see above). The position of O2′ is occupied in subunit *D* by a third water molecule [Water(3)] which is hydrogen-bonded to the Glu197 $O^{\varepsilon 1}$ atom. Water(4) does not mimic any Ado atom, but is involved in hydrogen bonding to the His392 N atom and in this way completes the active-site architecture of subunit *D*. In addition, the side chain of Gln62 is shifted into the active site in the ligand-free subunit, placing its $O^{\varepsilon 1}$ atom in the position of the Ado N6 atom in the Ado complex.

3.4. Ligand-induced conformational change

Ado molecules were found in subunits *A*, *B* and *C*, but not in subunit *D*. Hu *et al.* (1999) showed that ligand binding in the active site of SAHase switches the subunit conformation from open to closed. In agreement with this observation, the subunits of the BeSAHase homotetramer are found in two conformational states: while the Ado-binding subunits *A*, *B* and *C* are in the closed conformation, the *D* subunit is open. The differences in terms of C^{α} r.m.s. deviations are shown in Table 4. Despite the difference in the overall conformation of the complexed and ligand-free subunits, the folds of the individual domains are the same, as illustrated by the small r.m.s.d. values calculated for C^{α} superpositions of subunits *A* and *D*, which are 0.32, 0.15 and 0.39 Å for the substrate-binding, cofactor-binding and dimerization domains, respectively. This indicates that there should be a region between the

Table 5
Main-chain torsion angles (°) in subunits *A* (closed form) and *D* (open form) that undergo the most pronounced change ($|\Delta| > 10°$) upon domain movement.

Because of the similarity of subunits *A*, *B* and *C*, only values for subunit *A* are given. $|\Delta|$ changes in excess of 20° are shown in bold. The two hinge regions are separated by a line.

Residue No.	Torsion angle	Subunit *A*	Subunit *D*	$\|\Delta\|$
222	ω	178.7	−169.6	11.7
223	ψ	5.0	−11.2	16.2
223	$\boldsymbol{\omega}$	**161.5**	**−174.1**	**24.4**
224	φ	−58.2	−69.7	11.5
224	ψ	139.6	155.1	15.6
226	$\boldsymbol{\psi}$	**1.8**	**−36.8**	**38.6**
226	ω	168.7	−179.2	10.5
227	$\boldsymbol{\varphi}$	**−109.8**	**−71.7**	**38.1**
227	ψ	−64.0	−50.8	13.2
229	$\boldsymbol{\varphi}$	**−95.7**	**−65.7**	**30.0**
229	$\boldsymbol{\psi}$	**10.6**	**−41.1**	**51.7**
230	$\boldsymbol{\varphi}$	**−127.0**	**−75.1**	**51.9**
230	$\boldsymbol{\psi}$	**−66.1**	**−44.3**	**21.8**
232	$\boldsymbol{\varphi}$	**−71.5**	**−98.9**	**27.4**
232	ψ	−35.4	−50.1	14.7
392	ψ	147.6	136.5	11.1
395	ψ	−48.7	−37.7	11.0
396	ψ	−32.2	−43.1	10.8

substrate-binding and cofactor-binding domains that functions as a hinge in the conformational transition. A comparison of the main-chain torsion angles of the open and closed subunits identifies the Asn222–Leu233 and His392–Val396 segments as the hinge regions, where the Ramachandran torsion angles differ by 13 and 7° on average, with maximum changes of 52 and 11°, respectively (Table 5). This indicates that the first hinge region is far more flexible and plays a key role in the conformational transition.

The fact that the Ado molecules were modelled with an occupancy of 0.7 implies that 30% of the *A*/*B*/*C* subunits in the crystal lattice are apparently not occupied by the Ado ligand. Nevertheless, these subunits seem to be uniformly in the closed conformation, as there was no indication whatsoever in the electron density of dual conformation or disorder. Also, a C^{α} comparison with LlSAHase in a 1:1 complex with Ado (see §3.10) shows that BeSAHase subunits *A*/*B*/*C* adopt a fully closed conformation. This would suggest that while binding of Ado (or a similar ligand) induces the closed conformation by necessity, this conformational state may also be assumed without a ligand (Zheng *et al.*, 2015), for instance upon stabilization by crystal-packing interactions.

3.5. The molecular gate to the active site

Reddy *et al.* (2008) showed that in the SAHase from *M. tuberculosis* His363 acts as a 'molecular gate' which opens and closes an access channel leading to the active site upon domain movement by rotating its side chain by ∼180° around the backbone. In the BeSAHase structure, movement of the His342 side chain (corresponding to His363 in *M. tuberculosis* SAHase) is coupled with a rotation of the Phe343 side chain, and these residues together form a two-part access-channel gate (Fig. 3) which is closed upon adenosine binding (subunits *A*, *B* and *C*) and open in subunit *D* (Fig. 2). Strictly speaking, the access channel of BeSAHase is shut in the subunits in the closed conformation, because its closure in protomers *A*/*B*/*C* seems to be insensitive to whether the Ado ligand is physically present (70%) or not (30%). In the recently reported structures of the plant SAHase from *L. luteus* (LlSAHase; Brzezinski *et al.*, 2012) the gate formed by the side chains of His350 (corresponding to His342 in BeSAHase) and Phe351 (corresponding to Phe343) was closed or open depending on the ligand molecule bound in the

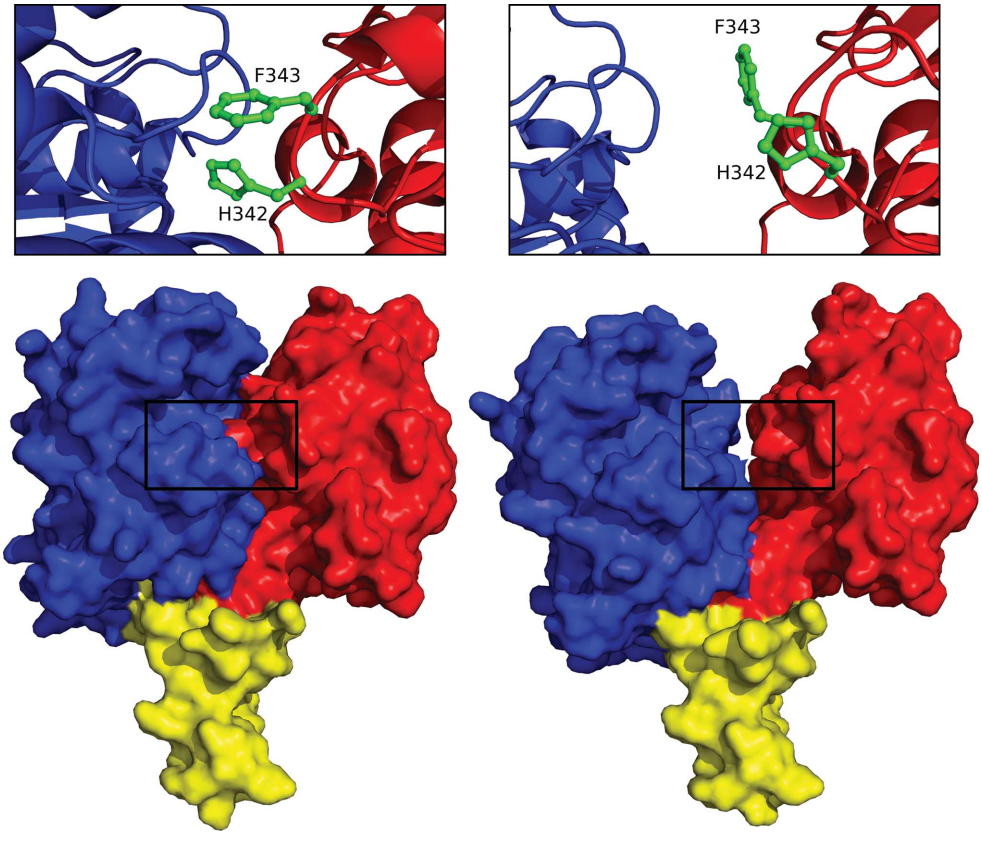

Figure 3
BeSAHase subunits in the closed (left) and open (right) conformation. The domains are coloured as follows: blue, substrate-binding domain; red, cofactor-binding domain; yellow, C-terminal oligomerization domain. The side chains of His342-Phe343, forming the molecular gate at the passage to the active site, are highlighted in the enlargements.

active site, but in a way that is inconsistent with the situation in BeSAHase. With adenosine or 3′-deoxyadenosine (cordycepin) bound, the side chains of the molecular gate were swung open, while access to the active site was blocked by these side chains only in the complex with adenine. It is interesting to note that the opening of the access gate with the Ado molecule still in the active site (as in LlSAHase) is accompanied by disruption of one of the hydrogen bonds (from the gate His residue to O5′) that anchor the product molecule in the active site. In general, only plasmodial and plant SAHases have the molecular gate open in Ado-complexed forms, while in all eukaryotic and bacterial enzymes the access channel is closed upon Ado binding. The only exception is SAHase from *M. tuberculosis* in complex with SAH (Reddy *et al.*, 2008; PDB entry 3dhy), in which the side chain of His363 is shifted to a different position to avoid a steric clash with the Hcy moiety. The picture emerging from these structures suggests that upon substrate (SAH) binding the enzyme assumes the closed conformation but the access channel cannot be fully closed because of collision with the Hcy fragment. As the reaction progresses, the Hcy product dissociates from the active site in concert with full closure of the gate. This is the conformational state of the Ado-bound subunits of the BeSAHase structure. In the next phase, the gate opens (as in LlSAHase) to allow release of the Ado product, which is accompanied by the transition of the enzyme to the final open conformation, as seen in the 'empty' subunit *D* of the BeSAHase structure.

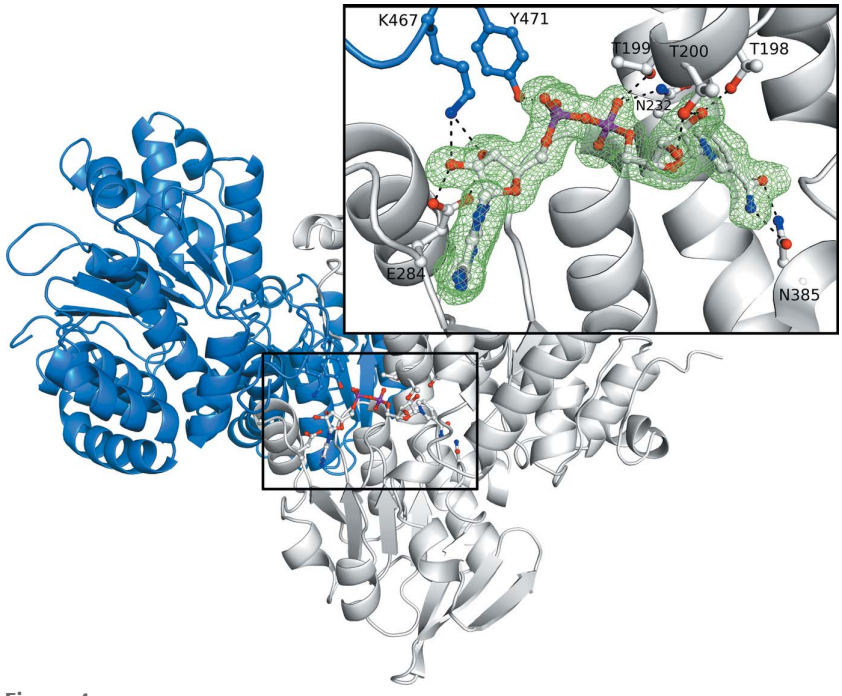

Figure 4
The intimate dimer of BeSAHase subunits *A* (grey) and *B* (blue) formed with the participation of the NAD^+ cofactor, shown in an $F_o - F_c$ OMIT electron-density map (calculated without the contribution of the NAD^+ atoms to F_c) contoured at the 3σ level (corresponding to 0.17 e Å^{-3}). For clarity, only selected hydrogen bonds (dashed lines) involving protein side chains are shown. All contacts are listed in Table 7.

3.6. Quaternary interactions between the subunits

Since the BeSAHase tetramer should be considered as a dimer of dimers, the majority of the intramolecular interactions occur between the intimate dimer-forming subunits *AB* (and also *CD*). Almost all of the interactions between these subunits are formed by residues from the cofactor-binding (Tyr234–Gly391) and C-terminal (Leu427–Tyr473) domains. The exceptions are the hydrophobic interactions involving His203 from the substrate-binding domain. In the *AB* dimer there are eight such contacts out of the 271 hydrophobic interactions (six involving His203 from subunit *A* and two His203 from subunit *B*). In the *CD* dimer, five of the 259 hydrophobic interactions are formed exclusively by His203 from subunit *C*. The borderline asymmetry within the dimers is explained by the (generally slight) conformational differences between the individual subunits and the hydrophobic interaction cutoff distance set at 3.9 Å in the *PDBsum* server (Laskowski, 2009).

In the *AB* dimer there are 26 hydrogen bonds between the protomers. Among them there are four that are not present in the *CD* dimer: Glu296*A* $O^{\varepsilon2}\cdots O^{\eta}$ Tyr234*B*, Arg451*A* $N^{\eta1}\cdots$ O Asp321*B*, Arg472*A* $O\cdots N^{\zeta}$ Lys229*B* and Tyr473*A* $O\cdots N^{\zeta}$ Lys229*B*. Also, two interactions in the *A*$\cdots$*B* direction are unique and are not present in the opposite *B*$\cdots$*A* direction: Arg452*A* $N^{\eta1}\cdots$O Asp321*B* and Arg472*A* $O\cdots N^{\zeta}$ Lys229*B*. In the *CD* dimer there are 24 hydrogen bonds between the subunits, among which the Lys320*C* $N^{\zeta}\cdots O^{\delta2}$ Asp453*D* and Arg472*C* $N^{\eta2}\cdots$O Asp223*D* interactions are unique to this dimer. The Lys229*C* $N^{\zeta}\cdots$O Tyr473*D*, Tyr234*C* $O^{\eta}\cdots O^{\varepsilon2}$ Glu296*D*, Lys320*C* $N^{\zeta}\cdots O^{\delta2}$ Asp453*D* and Arg472*C* $N^{\eta2}\cdots$O Asp223*D* interactions are present only in the *C*$\cdots$*D* direction. As seen from this hydrogen-bond inventory, the conformational state of the subunits does not significantly affect the number of interactions between them in the intimate dimers and the presence of Ado molecules in the active site is not required for dimer formation.

Among the numerous hydrogen bonds and hydrophobic contacts, the most crucial for dimer formation seem to be the interactions formed by the small dimerization domain at the C-terminus. Two residues from this domain, Lys467 and Tyr471, are involved in cofactor binding in the complementary subunit (Fig. 4). Lys467 forms two hydrogen bonds using its N^{ζ} atom to O2B and O3B of the NAD^+ molecule. Tyr471 O^{η} forms a hydrogen bond to the O1A atom of the cofactor (for NAD^+ atom numbering, see Fig. 5). This way, the complete cofactor-binding site is created with the participation of both protomers forming the tight dimer. Ault-Riché *et al.* (1994) showed that mutation of Lys426 in human SAHase (corresponding to Lys467 in BeSAHase) to alanine or glutamate

Table 6
Interaction interfaces between the subunits forming the BeSAHase tetramer, calculated with *PDBsum* (Laskowski, 2009).

N_r, number of interface residues; N_h, number of hydrogen bonds; N_{nbc}, number of nonbonded contacts.

Protein chains	N_r	N_h	N_{nbc}	Interface area (Å^2)
A:*B*	51:52	26	271	2975:2960
C:*D*	49:49	24	259	2832:2818
A:*C*	31:31	26	187	1685:1693
B:*D*	28:28	26	173	1593:1608
A:*D*	7:7	0	23	370:367
B:*C*	8:8	0	20	386:386

resulted in inactive, monomeric protein without the cofactor.

The numbers of interactions between subunits that do not form tight dimers (*e.g. A*–*C*, *A*–*D etc.*) are smaller than in the cases described above. Contacts between subunits that are juxtaposed in Fig. 1 (*A*–*C* and *B*–*D*) are formed by residues from all domains. Nevertheless, there are 26 hydrogen bonds in each pair involving amino-acid residues from the substrate-binding and cofactor-binding domains. However, the number of hydrophobic contacts is much smaller than in the tight dimers, with 187 hydrophobic interactions in the *A*–*C* pair and 173 in the *B*–*D* pair, with the involvement of only one residue from the C-terminal domain: Ile443 from subunit *A* or *B*.

The remaining pairs within the homotetramer, *i.e. A*–*D* and *B*–*C*, form no hydrogen bonds. There are only 23 hydrophobic

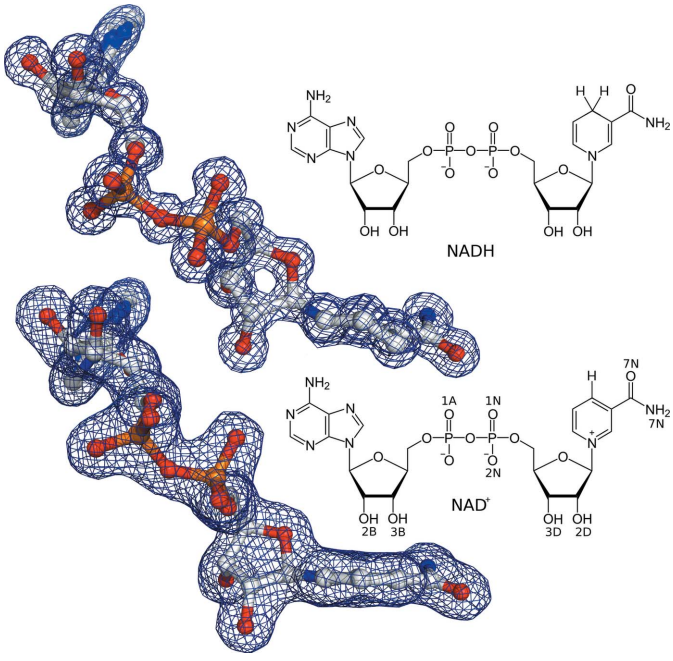

Figure 5
The molecule of NADH (top) from the PDB structure 1het (Meijers *et al.*, 2001) and NAD$^+$ (bottom) from the present BeSAHase structure (subunit *A*). The difference in the puckering of the nicotinamide ring indicates the oxidation state of each molecule, shown in $2F_o - F_c$ electron density contoured at 1σ, which corresponds to 0.72 e Å^{-3} for NADH and 0.48 e Å^{-3} for NAD$^+$. The chemical formulae illustrate the principal electronic forms of the molecules and the numbering of some key atoms of NAD$^+$.

Table 7
Hydrogen-bond interactions between the cofactor NAD$^+$ molecule and protein atoms.

Because of the similarity of all four cofactor-binding sites, only values for NAD$^+$ bound in subunit *A* are shown. The last three rows show interactions with amino-acid residues from the complementary subunit (*B*) of the tight dimer. The NAD$^+$ atom-labelling scheme is introduced in Fig. 5.

Residue No. and atom	NAD$^+$ atom	Distance (Å)
Thr198 $O^{\gamma1}$	O2D	2.76
Thr199 $O^{\gamma1}$	O1N	2.73
Thr200 N	O2D	3.21
Thr200 $O^{\gamma1}$	O2D	3.34
Thr200 $O^{\gamma1}$	O3D	2.67
Asn232 $N^{\delta2}$	O1N	3.32
Val265 N	O2N	2.87
Glu284 $O^{\varepsilon1}$	O3B	2.78
Glu284 $O^{\varepsilon2}$	O2B	2.66
Ile340 O	N7N	2.81
His342 N	O3D	3.09
Asn385 $O^{\delta1}$	N7N	3.10
Asn385 $N^{\delta2}$	O7N	2.92
Lys467(*B*) N^{ζ}	O2B	3.10
Lys467(*B*) N^{ζ}	O3B	2.84
Tyr471(*B*) O^{η}	O1A	2.54

interactions in the former case and 20 in the latter. These contacts involve residues from the substrate-binding domains only. Detailed information about the protein–protein interactions within the homotetramer is summarized in Table 6.

3.7. Crystal packing and interactions between the tetramers

BeSAHase crystallized in space group $P2_12_12$ with four protein molecules forming the complete 222 pseudosymmetric tetramer in the asymmetric unit (Fig. 1). Although this space group contains point symmetry compatible with the molecular symmetry of the enzyme, it is not utilized by the tetramer in the asymmetric unit. The pseudo-twofold molecular axis that relates subunits *A* to *D* (and *B* to *C*) is nearly parallel (3.3° inclination) to the [100] direction. The remaining molecular axes are not aligned with crystallographic directions.

PISA (Krissinel & Henrick, 2007) analysis revealed that the largest interaction area between symmetrically equivalent protein molecules is less than 500 Å^2. This value is comparable with the interfaces between subunits with a diagonal disposition across the tetramer (*A*–*D* and *B*–*C*; Table 6).

3.8. The cofactor: mode of binding and oxidation state

The cofactor-binding site is highly conserved in all SAHases. Most of the interactions are provided by residues from the cofactor-binding domain. However, as described above, the C-terminal domain of the complementary subunit also participates in NAD$^+$ binding, at the same time providing the most important cohesive force for the intimate dimer. All cofactor interactions are listed in Table 7.

To support the conclusion about the oxidation state of the cofactor, we analyzed the puckering of the nicotinamide moiety. It has been shown by Meijers *et al.* (2001) that addition of hydride anion to the NAD$^+$ nicotinamide ring causes a loss of its aromatic character and its deformation into a boat conformation. To obtain an unbiased view, we refined the

Table 8
Hydrogen-bond distances around the ammonium ions in subunits *A*/*B*/*C*.

Ligand atom	Bond length (Å)
Met390 O	3.00/2.98/2.94
His392 O	3.16/3.09/3.08
Water(A)	2.59/2.37/2.53
Water(B)	2.78/2.89/2.92
Water(C)	2.98/3.09/2.94

Table 9
R.m.s. deviations (Å) for C^{α} atoms of superposed subunits of BeSAHase and RnSAHase in closed and open conformations calculated with *ALIGN* (Cohen, 1997).

	BeSAHase, closed	BeSAHase, open	RnSAHase, closed
BeSAHase, open	2.32		
RnSAHase, closed	0.75	2.05	
RnSAHase, open	2.14	0.97	2.12

NAD^+ molecules without planarity restraints and found that the nicotinamide ring of all of these moieties in the BeSAHase crystal structure is flat (Fig. 5). Thus, it can be concluded that the cofactor is in its oxidized NAD^+ state. The question about the cofactor oxidation state has a biochemical and an electrochemical aspect. We tried to address the former aspect by incubating the protein with a cofactor of uniform oxidation state (NAD^+; see §2.1). The latter aspect is connected to the belief that the X-ray beam (through generation of electrons) provides a strongly reducing milieu. However, in the crystal of BeSAHase this evidently did not lead to a noticeable effect.

3.9. Ammonium/metal cations and their role in structure stabilization

In the Ado-bound subunits *A*, *B* and *C*, an ammonium cation was found in the loop Ala389–Pro393 (Fig. 6) that links the substrate-binding and cofactor-binding domains and is located near the active site of the enzyme. The last two residues of this loop, His392 and Pro393, are also part of the second hinge region. This loop corresponds to the Ala401–Pro405 loop of LlSAHase from *L. luteus*, which was also shown to bind a sodium cation (Brzezinski *et al.*, 2012) in the closed form of the subunits. The ammonium ion was present at a relatively high concentration (0.2 *M*) in the crystallization buffer. Its identification is based on the hydrogen-bond distances (Table 8) and was additionally validated by the calcium bond-valence sum method (Müller *et al.*, 2003). In the pattern of interactions, the NH_4^+ ion forms hydrogen bonds to five O acceptors (including three water molecules), meaning that one of the NH donors forms a bifurcated hydrogen bond. No cationic species were found in the Ala389–Pro393 loop of the open subunit *D*, but a poorly bound water molecule is situated near the carbonyl group of Met390.

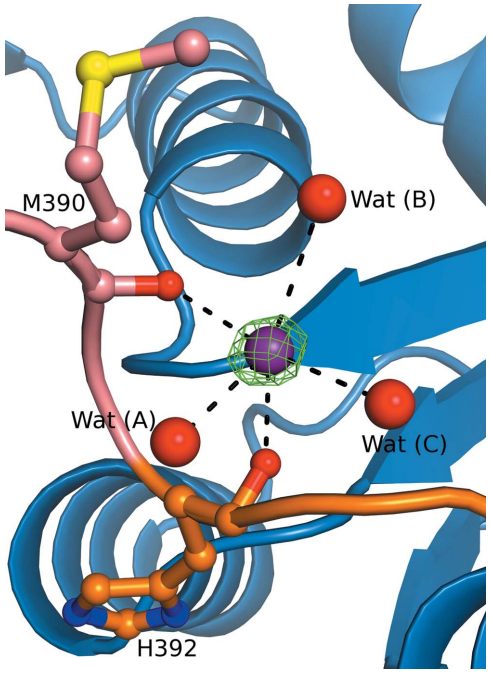

Figure 6
The ammonium ion (violet sphere) bound in subunit *A*, shown in $F_o - F_c$ OMIT electron density (calculated without the contribution of the NH_4^+ atoms to F_c) contoured at 5σ (corresponding to 0.27 e Å^{-3}). Hydrogen-bond (dashed lines) details are listed in Table 8. Water molecules are represented as red spheres. The domains are colour-coded as follows: blue, substrate-binding domain; salmon, cofactor-binding domain. Orange colour represents the second hinge region between these domains.

The presence of the ammonium ion only in those subunits that have Ado molecules bound in the active site and are in the closed conformation may suggest that it is important for stabilizing this conformation. It was shown by Yin *et al.* (2000) that the cofactor-binding and substrate-binding domains are mobile until ligand binding. Wang *et al.* (2006) in turn showed that the mutation of His353 in human SAHase (corresponding to His392 in BeSAHase that takes part in NH_4^+ binding) to alanine slowed down the domain mobility. The structure of BeSAHase sheds new light on this aspect, showing that the closed-conformation ligand-bound state is additionally stabilized by a cation bound in a loop linking the cofactor-binding and substrate-binding domains. Apparently, the ion bound in this loop can be either an alkali-metal cation, as in LlSAHase (Na^+) and in SAHase from *B. melitensis* (K^+), or NH_4^+, as in BeSAHase.

3.10. BeSAHase *versus* other SAHases: conformational analysis

Among the SAHase models deposited in the PDB, BeSAHase is the first structure in which two conformational states of the enzyme are present in one crystal. SAHase from *R. norvegicus* (RnSAHase) is the only protein for which structures in the open (Hu *et al.*, 1999; PDB entry 1b3r) and closed (Ado complex; Komoto *et al.*, 2000; PDB entry 1d4f) conformations have been observed, but in distinct crystal structures. Superpositions of the C^{α} traces (Table 9) show that the differences between the open and closed conformations are the same in both proteins, with corresponding r.m.s.d. values of 2.32 and 2.12 Å for BeSAHase and RnSAHase, respectively. Comparison of the closed and open subunits of the two enzymes shows that protomers in the same confor-

mational state are quite similar, with r.m.s.d. values of 0.75 and 0.97 Å, respectively. This shows that the open-closed conformational transition is structurally conserved among SAHases from different organisms. Also, when the closed subunits of BeSAHase are compared with the closed subunits of SAHases from other organisms, *L. luteus*, *B. melitensis* (both in complex with Ado) and from *H. sapiens* in complex with neplanocin, a high degree of structural conservation is revealed, with C^{α} r.m.s.d. values of 0.51, 0.33 and 0.64 Å, respectively.

4. Conclusions

The crystal structure of SAHase from *B. elkanii* was solved at a resolution of 1.74 Å, revealing a homotetramer in the asymmetric unit of space group $P2_12_12$. Although only NAD^+ molecules were deliberately added during protein preparation and crystallization, molecules of Ado, which is one of the products of the reaction catalyzed by SAHase, were found in the electron-density maps in three of the four subunits of the tetrameric enzyme. The *A*, *B* and *C* subunits, in which the Ado product is bound, have a closed conformation, in contrast to the 'empty' subunit *D*, which is open. In the closed conformation, the substrate-binding and cofactor-binding domains are brought together to allow the catalytic reaction to proceed. The structure clearly shows that transition between the open and closed states requires a significant conformational change of a hinge segment of five residues and is coupled to a conformational switch of two gating residues (His342 and Phe343), which control access to the active site. In addition, the closed conformation is stabilized by an NH_4^+ cation bound in a loop connecting the substrate-binding and cofactor-binding domains. The identity of the bound cation, consistent with the high concentration of NH_4^+ in the crystallization buffer, was confirmed by the pattern of hydrogen-bond distances and the calcium bond-valence sum method (Müller *et al.*, 2003). In other SAHases studied in the closed conformation, the cation-binding loop coordinates an alkali-metal ion. In each subunit, there is clear electron density indicating the presence of the NAD^+ cofactor, the oxidation state of which is confirmed by the flat (no puckering) nicotinamide ring. The cofactor-binding site of subunit *A* is complemented in a mutual fashion by residues from the C-terminal oligomerization domain of subunit *B*, and an analogous relation exists between subunits *C* and *D*. Owing to these interactions, the tetrameric enzyme should be considered as a dimer of two tight dimers (*AB* and *CD*).

Acknowledgements

This work was supported in part by the Ministry of Science and Higher Education KNOW program. The project was co-funded by the European Union within the European Regional Development Fund. MJ is a recipient of National Science Center grant 2013/10/M/NZ1/00251.

References

Adams, P. D. *et al.* (2010). *Acta Cryst.* D**66**, 213–221.
Ault-Riché, D. B., Yuan, C.-S. & Borchardt, R. T. (1994). *J. Biol. Chem.* **269**, 31472–31478.
Bradford, M. M. (1976). *Anal. Biochem.* **72**, 248–254.
Brzezinski, K., Bujacz, G. & Jaskolski, M. (2008). *Acta Cryst.* F**64**, 671–673.
Brzezinski, K., Dauter, Z. & Jaskolski, M. (2012). *Acta Cryst.* D**68**, 218–231.
Cantoni, G. L. (1975). *Annu. Rev. Biochem.* **44**, 435–451.
Cantoni, G. L. & Chiang, P. K. (1980). *Natural Sulfur Compounds*, pp. 67–80. New York: Plenum.
Chiang, P. K. & Cantoni, G. L. (1979). *Biochem. Pharmacol.* **28**, 1897–1902.
Cohen, G. H. (1997). *J. Appl. Cryst.* **30**, 1160–1161.
De La Haba, G. & Cantoni, G. L. (1959). *J. Biol. Chem.* **234**, 603–608.
DeLano, W. L. (2002). *PyMOL*. http://www.pymol.org.
Emsley, P. & Cowtan, K. (2004). *Acta Cryst.* D**60**, 2126–2132.
Fujioka, M. & Takata, Y. (1981). *J. Biol. Chem.* **256**, 1631–1635.
Guranowski, A. & Pawełkiewicz, J. (1977). *Eur. J. Biochem.* **80**, 517–523.
Hershfield, M. S. (1979). *J. Biol. Chem.* **254**, 22–25.
Hershfield, M. S., Kredich, N. M., Ownby, D. R., Ownby, H. & Buckley, R. (1979). *J. Clin. Invest.* **63**, 807–811.
Hershfield, M. S. & Kredich, N. M. (1978). *Science*, **202**, 757–760.
Hu, Y., Komoto, J., Huang, Y., Gomi, T., Ogawa, H., Takata, Y., Fujioka, M. & Takusagawa, F. (1999). *Biochemistry*, **38**, 8323–8333.
Huang, Y., Komoto, J., Takata, Y., Powell, D. R., Gomi, T., Ogawa, H., Fujioka, M. & Takusagawa, F. (2002). *J. Biol. Chem.* **277**, 7477–7482.
Jaskólski, M. (1984). *Acta Cryst.* A**40**, 364–366.
Kabsch, W. (2010). *Acta Cryst.* D**66**, 125–132.
Keller, B. T. & Borchardt, R. T. (1988). *Antivirial Drug Development: A Multidisciplinary Approach*, edited by E. De Clerq & R. T. Walker, pp. 123–138. New York: Plenum.
Komoto, J., Huang, Y., Gomi, T., Ogawa, H., Takata, Y., Fujioka, M. & Takusagawa, F. (2000). *J. Biol. Chem.* **275**, 32147–32156.
Kredich, N. M. & Martin, D. W. Jr (1977). *Cell*, **12**, 931–938.
Krissinel, E. & Henrick, K. (2007). *J. Mol. Biol.* **372**, 774–797.
Langer, G., Cohen, S. X., Lamzin, V. S. & Perrakis, A. (2008). *Nature Protoc.* **3**, 1171–1179.
Laskowski, R. A. (2009). *Nucleic Acids Res.* **37**, D355–D359.
Liu, S., Wolfe, M. S. & Borchardt, R. T. (1992). *Antiviral Res.* **19**, 247–265.
McCoy, A. J., Grosse-Kunstleve, R. W., Adams, P. D., Winn, M. D., Storoni, L. C. & Read, R. J. (2007). *J. Appl. Cryst.* **40**, 658–674.
McKeever, M. P., Weir, D. G., Molloy, A. & Scott, J. M. (1991). *Clin. Sci.* **81**, 551–556.
Meijers, R., Morris, R. J., Adolph, H. W., Merli, A., Lamzin, V. S. & Cedergren-Zeppezauer, E. S. (2001). *J. Biol. Chem.* **276**, 9316–9321.
Mitsui, S., Wakasugi, T. & Sugiura, M. (1993). *Plant Cell Physiol.* **34**, 1089–1096.
Moriarty, N. W., Grosse-Kunstleve, R. W. & Adams, P. D. (2009). *Acta Cryst.* D**65**, 1074–1080.
Müller, P., Köpke, S. & Sheldrick, G. M. (2003). *Acta Cryst.* D**59**, 32–37.
Murshudov, G. N., Skubák, P., Lebedev, A. A., Pannu, N. S., Steiner, R. A., Nicholls, R. A., Winn, M. D., Long, F. & Vagin, A. A. (2011). *Acta Cryst.* D**67**, 355–367.
Nygård, O., Nordrehaug, J. E., Refsum, H., Ueland, P. M., Farstad, M. & Vollset, S. E. (1997). *N. Engl. J. Med.* **337**, 230–237.
Painter, J. & Merritt, E. A. (2006). *Acta Cryst.* D**62**, 439–450.
Palmer, J. L. & Abeles, R. H. (1976). *J. Biol. Chem.* **251**, 5817–5819.
Palmer, J. L. & Abeles, R. H. (1979). *J. Biol. Chem.* **254**, 1217–1226.
Reddy, M. C., Kuppan, G., Shetty, N. D., Owen, J. L., Ioerger, T. R. & Sacchettini, J. C. (2008). *Protein Sci.* **17**, 2134–2144.
Richards, H. H., Chiang, P. K. & Cantoni, G. L. (1978). *J. Biol. Chem.* **253**, 4476–4480.
Robinson, K., Mayer, E. & Jacobsen, D. W. (1994). *Cleve. Clin. J. Med.* **61**, 438–450.

Stępkowski, T., Brzeziński, K., Legocki, A. B., Jaskólski, M. & Béna, G. (2005). *Mol. Phylogenet. Evol.* **34**, 15–28.
Takata, Y., Yamada, T., Huang, Y., Komoto, J., Gomi, T., Ogawa, H., Fujioka, M. & Takusagawa, F. (2002). *J. Biol. Chem.* **277**, 22670–22676.
Tanaka, N., Nakanishi, M., Kusakabe, Y., Shiraiwa, K., Yabe, S., Ito, Y., Kitade, Y. & Nakamura, K. T. (2004). *J. Mol. Biol.* **343**, 1007–1017.
Turner, M. A., Yuan, C.-S., Borchardt, R. T., Hershfield, M. S., Smith, G. D. & Howell, P. L. (1998). *Nature Struct. Biol.* **5**, 369–376.
Wang, M., Unruh, J. R., Johnson, C. K., Kuczera, K., Schowen, R. L. & Borchardt, R. T. (2006). *Biochemistry*, **45**, 7778–7786.
Yang, X., Hu, Y., Yin, D. H., Turner, M. A., Wang, M., Borchardt, R. T., Howell, P. L., Kuczera, K. & Schowen, R. L. (2003). *Biochemistry*, **42**, 1900–1909.
Yin, D., Yang, X., Hu, Y., Kuczera, K., Schowen, R. L., Borchardt, R. T. & Squier, T. C. (2000). *Biochemistry*, **39**, 9811–9818.
Zheng, Y., Chen, C.-C., Ko, T.-P., Xiao, X., Yang, Y., Huang, C.-H., Qian, G., Shao, W. & Guo, R.-T. (2015). *J. Struct. Biol.* **190**, 135–142.